Fourier Transforms of μSR Data and Their Use in the the Determination of the Internal Magnetic Field Distributions of $YBa_2Cu_3O_{7-\delta}$

Aaron Suplizio

Advisor: W.J. Kossler

May 9, 2000

Abstract

Field distributions from muon spin rotation experiments are obtained by taking the Fourier transform of precession data. Several different techniques to carry out these transforms have been developed and tested using data from single crystals of the high T_c superconductor $YBa_2Cu_3O_{7-\delta}$, which had inclusions of non-superconducting material. These techniques were: cosine transforms carried out as a sum over the data and a range of frequencies, least-squares fits to cosine amplitudes, least-squares fits to cosine amplitudes represented as exponentials, and finally with a maximum entropy technique. All produced similar results. These cosine amplitudes will be used in the future to study disorder and melting of the vortex lattice.

Introduction

Determining the physical properties of superconductors requires investigating the internal magnetic field distributions of the material in question. Dr. Kossler and I are analyzing data taken from the TRIUMF Lab at the University of British Columbia. Using the techniques of muon spin rotation (μSR), we have produced time-spectrum histograms of muon decay in the high T_c superconductor $YBa_2Cu_3O_{7-\delta}$ (YBCO) at various fields and temperatures. Fourier transforms of the asymmetry representations of this data yield the internal magnetic field probability distributions of the YBCO, and we have performed such transforms in four different ways. We next review relevant properties of superconductors so as to put the Fourier analysis results in context. The methodologies and results are then discussed, followed by comparisons of the various techniques.

Superconductivity

There are two universal parameters used to describe superconducting materials. The first is known as the *penetration depth*, λ [4, 5]. The penetration depth is a measure of how quickly the magnetic fields in superconductors decay. The second parameter is the *coherence length*, ξ. This constant measures the distance at which the local magnetic fields have a significant effect on the current at some other point. Superconductors are classified into two different types according to the ratio $\kappa \equiv \frac{\lambda}{\xi}$, where κ is known as the Ginzburg-Landau factor. A Type I superconductor has $\kappa < \frac{1}{\sqrt{2}}$, whereas a Type II superconductor has $\kappa > \frac{1}{\sqrt{2}}$. Pb, Sn, and Al are all examples of classic, Type I superconductors. For temperatures below the

critical temperature T_c and below some critical field H_c, the magnetic field behavior curve will be linear with a slope of 1. That is, a Type I superconductor will completely expel the magnetic field to which it is being subjected according to the Meissner effect for fields below H_c. When the external magnetic field is made greater than H_c, there is an abrupt transition to the normal conducting state, and the external magnetic field is completely allowed within the material.

The situation is slightly different for a Type II superconductor, which will have two critical field values: H_{c1} and H_{c2}. For fields below H_{c1}, the field will be completely expelled from the superconductor. There is, however, a transitional stage for the region between H_{c1} and H_{c2}. Here, a mixed state is achieved where the external magnetic field is allowed to penetrate more as its strength is increased. When the upper limit H_{c2} is finally reached, the field can penetrate the superconductor completely, and the material reverts back to having its normal conducting properties.

When a material is in the mixed state mentioned above, the magnetic flux penetrates in units of the flux quantum $\Phi_0 = \frac{hc}{2e} = 2.07 \cdot 10^{-7} G \cdot cm^2$. It has been demonstrated that a triangular flux line lattice is often the proper one for minimizing the free energy of a system, and the resulting equilibrium geometry places a flux quantum or vortex at each of the vertices of the triangles in this lattice.

Using the results of isotropic London theory, one can obtain the equations for theoretically determining the magnetic field among these vortices. Outside of a singular vortex and isolated from the effects of other vortices in the aforementioned lattice, one can see that the magnetic field dies off exponentially as the distance measured from the vortex tends towards

infinity.

The practical case where an array of vortices exists can be described by solving the equation

$$b_z = \lambda_L^2 \nabla \times (\nabla \times \mathbf{b}) = \Phi_0 \delta(r - r_v) \tag{1}$$

which yields

$$b_z(\vec{r}) = \frac{\Phi_0}{2\pi\lambda^2} K_0(r/\lambda) \tag{2}$$

where $K_0(x)$ is a zero-order Bessel function of imaginary arguments.

Considering another simplified scenario can lend insight as to the geometry of the magnetic fields between the vortices. Taking just two vortices separated by some small distance with V_1 on the left and V_2 on the right, the magnetic field would die off exponentially to the right of V_1 and to the left of V_2: because the distribution is continuous the two fields must meet at some point.

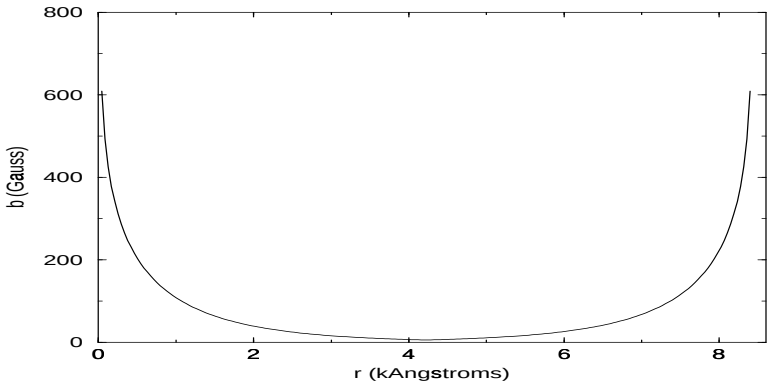

Figure 1: The magnetic field distribution between two adjacent vortices. V_1 is located at the origin, V_2 is located approximately 8.5 kAngstroms away.

There obviously exists some kind of minima between adjacent vortices. Extending this example to a triangular lattice of flux quanta, one can picture the magnetic field distribution to be "hilly," with saddle points and minima and valleys between the vortices. One is referred to the monogram of Kossler for three-dimensional plots of such distributions.

The Technique of μSR

The "R" in the acronym μSR can stand for 1) resonance, 2) relaxation, or 3) rotation, among other "R's". Muon spin resonance is so named in analogy to nuclear magnetic resonance (NMR). In a certain branch of μSR called RF- μSR, a sample is placed in a Radio Frequency electromagnetic field. This field induces transitions among the hyperfine energy levels of the muon. When the magnetic field assumes certain values, there is an overall reduction in the decay asymmetry, which allows for a local determination of the hyperfine energy levels in the muon's environment [2]. Muon spin relaxation refers to techniques that measure the spin-lattice relaxation rate. The acronym most relevant to this discussion is muon spin rotation, where rotation refers to the precession of the muon's spin magnetic moment about the local magnetic field where it sits. This rotation is a result of basic electrodynamics. The muon's moment experiences a torque in a magnetic field:

$$\boldsymbol{\tau} = \boldsymbol{\mu} \times \mathbf{B}. \tag{3}$$

τ is defined to be the torque, and hence, the spin-angular momentum. So, this τ will give rise to a precession of the spin-magnetic moment of the muon in a local magnetic field B.

The magnetic moment of the muon is defined by:

$$\boldsymbol{\mu} = \gamma \mathbf{S} \tag{4}$$

where γ is the gyromagnetic ratio of the spin in question. Plugging Eq. 4 into Eq. 3 above, we obtain:

$$\frac{d\mathbf{S}}{dt} = \gamma \mathbf{S} \times \mathbf{B} \tag{5}$$

which defines the precession of the moment about the field.

There are several unique characteristics of the muon itself which permit μSR to work. First, there is a violation of parity in muon production. This motivates the decay of the muon into a positron in the direction of the muon's spin. The corresponding neutrinos' spins are anti-aligned, and thus the vectors sum to zero. Also of note is the perfect polarization of the muon's spin–that is, its spin is perfectly anti-aligned with its momentum. These features allow for several critical measurements to be determined, and will be discussed in the following section discussing the basic technique of μSR [2].

Of obvious importance is an accelerator to produce positive pions. Several reactions between proton beams and target protons yield these particles:

$$p + p \rightarrow p + n + \pi^+$$

$$p + n \rightarrow n + n + \pi^+$$

$$p + n \rightarrow p + n + \pi^-$$

The accelerator must supply an adequate amount of energy into each particle to create the desired reaction, in this case it is on the order of 500 MeV per proton. The current of the beam must also be relatively high, on the average about 100μA (about 1.6 quadrillion protons/second is on the low end of the requirements)[3]. The incident protons are fired into a production target (See Figure 2), and pions are produced. A number of these pions are stopped before reaching the outermost layer of the target. They then decay into muons and neutrinos according to the following reaction:

$$\pi^+ \rightarrow \mu^+ + \nu_\mu \tag{6}$$

Such particles are commonly called "surface muons" [3]. After a period of approximately 2-10 μs, the muon decays according to the three body reaction:

$$\mu^+ \rightarrow e^+ + \nu_e + \nu_\mu \tag{7}$$

It is now possible to follow the path of the muon into the sample whose properties we wish to study. The incoming muons follow the beamline until it passes through a thin counter (denoted M in Figure 2). This event produces a pulse which starts an electronic clock with time resolution better than $1 \cdot 10^{-9} s$. Due to the aforementioned parity violation, the muon arrives 100% spin polarized. After it decays, it tends to emit a positron (e^+) preferentially in the direction of its spin at the moment of decay. That positron is recorded by the e+ counters (marked F, B, L, R in Figure 2). The detection of the positron triggers the stop time for the clock. The time interval between the initial muon passing through the counter

and the corresponding positron is then recorded, and the count is added to a bin of a time histogram corresponding to that interval. This procedure is typically repeated for several million counts. The resulting time spectrum displays an exponential lifetime distribution of the muon, superimposed upon which is the probability of the positron being emitted in the direction of that detector. The precession of the muon will cause it to sweep periodically past the front and back detectors, creating a sinusoidal oscillation in time.

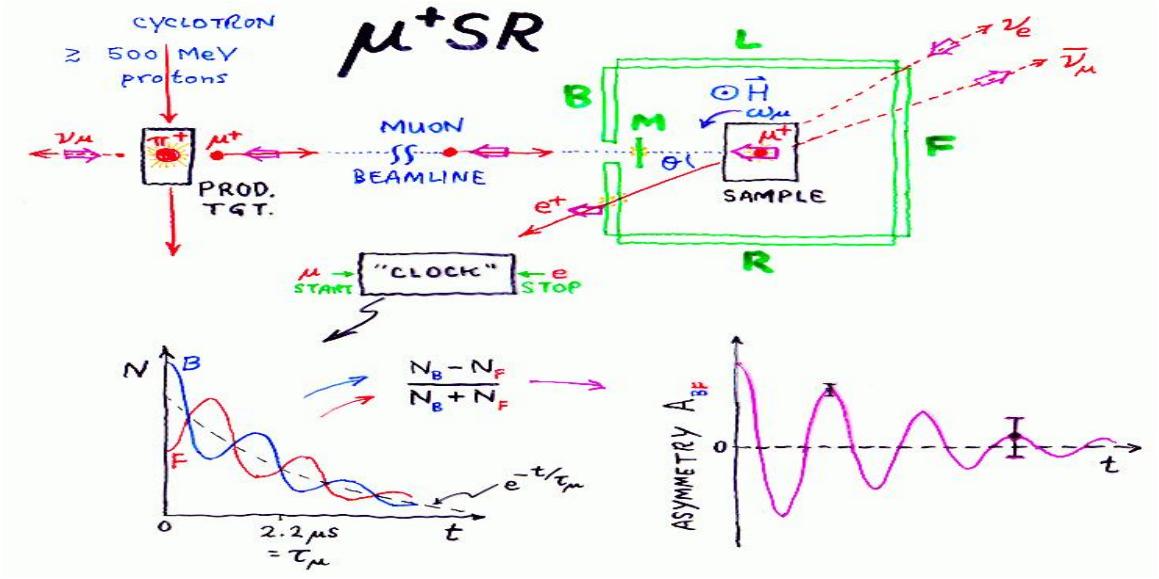

Figure 2: Counterclockwise from top, a sketch of the μSR apparatus, sample data taken from two opposing detectors, the asymmetry representation of the data.

There is a certain amount of dead time before the histogram starts recording actual events. It is during this empty time that the logic of the electronics tries to decide whether or not it has detected a muon. Generally, this part of the histogram is not displayed, but the data is used to determine the random background of each detector. This information turns out to be useful in preparing an asymmetry representation of the paired histogram data (that is, data combined from, say, the front (1) and back (2) detectors. Being on opposite ends,

the data from 1 and 2 are 180 degrees out of phase, but one can filter out their differences through the following relation:

$$asy(t) = \frac{(N_1 - B_1) - \alpha(N_2 - B_2)}{(N_1 - B_1) + \alpha(N_2 - B_2} \tag{8}$$

where N_1 and N_2 are the raw data from the histogram and B_1 and B_2 are the backgrounds. The experimentally determined α is a parameter meant to account for the efficiencies of the two detectors. Because of the division in the asymmetry function, *asy(t)* will no longer have the exponential fall-off associated with the muon's lifetime.

Fourier Analysis and Its Shortcomings

Given that we have data represented by histograms in the time domain, it turns out to be useful to translate it to the frequency domain. The link is found in Fourier analysis. The Fourier Transform of the data in the asymmetry representation is directly proportional to the internal magnetic field distributions of the material in question. Dr. Kossler and I have performed such transforms via several different implementations, hoping to find consistency among them. The methodology of each individual transform is not perfect, however, and there exist several shortcoming which require further discussion.

The first problem deals with data at time t = 0. This data is not accessible, which introduces problems in the Fourier analysis. The solution in this case is calls for an extrapolation of the data around t = 0 to create a best fit in that region. A fit to the data can be extended in the -t direction, creating a best fit at t=0. While this is a satisfactory solution, there

remain other problems that are not as trivial.

A second problem deals with the finite time range of the μSR data. Because the data are collected over a sum of discrete time intervals, the histogrammed plots do not necessarily go to zero at the endpoints of the time range. Fourier transforms require such behavior as t approaches infinity. Therefore, some measure must be take to ensure that the data does in fact tend to zero. The solution here is apodization. Apodization takes a certain relaxation function, such as a Gaussian, that decays to zero. The convolution of the data with the relaxation function now tends to zero as well. Depending on how quickly the relaxation function decays, it is possible to substantially reduce the oscillations that appear near the endpoints of the original function (such oscillations are known as "ringing") [3]. The negative effect of this treatment of the data is a broadening of the distribution in the frequency spectrum, which is directly proportional to the strength of the apodization.

The final technique to be implemented is a procedure called Maximum Entropy. It is a search scheme with many other applications, but on our data it produces results similar to a cosine transform. The technique depends on minimizing the expression:

$$\frac{1}{2}\chi^2[\mathbf{u}] + \sum_{\mu=\mathbf{1}}^{\mathbf{M}} \mathbf{u}_\mu \ln \frac{\mathbf{u}_\mu}{\mathbf{U}} \tag{9}$$

where $U = \sum_{\mu=1}^{M} u_\mu$, the u_μ are the Fourier amplitudes and the second summand is the negative of the "entropy". Maximum entropy theoretically gets rid of many of the aforementioned oscillations, increasing the resolution of the data.

Data Analysis

The above development leads us to the focus of my project. The material that is the focus of Dr. Kossler's research at TRIUMF and my data analysis is the aforementioned $YBa_2Cu_3O_{7-\delta}$ (YBCO). The efforts of research conducted at the University of Alabama and the University of Houston, YBCO was found to exhibit superconducting properties at a temperature of 92K[6]. This result stirred the scientific community not only because the highest critical temperature of any previously studied superconductor was on the order of 30-35K, but because 92K was significantly higher than the boiling point of liquid nitrogen–this made studying the properties of superconductivity more affordable and accessible.

At TRIUMF, a sample of YBCO was placed in various external magnetic fields and temperatures, then subjected to a muon beam according to the technique described earlier in this paper. The raw data from the decay of the muons was then put into the form of histograms. Dr. Kossler and I have utilized a FORTRAN program, TRI00, which performs many of the numerical operations necessary to extrapolate the magnetic field distributions of YBCO from the data.

My analysis was performed on a group of 26 data sets where the YBCO was subjected to external fields ranging from .5G to 107G, and temperatures ranging from 10K up to 91K, one degree below the critical temperature for YBCO. From this data, the goal was to produce an asymmetry plot created from two opposing detectors according to Eq. 8. The internal magnetic field distributions are linked to the asymmetry data via the following Fourier Transform:

$$asy(t) = \int_0^\infty \frac{dP(b)}{db} \cos(\gamma b \cdot t) dh \tag{10}$$

Where $\frac{dP(b)}{db}$ is given by:

$$\frac{dP(b)}{db} = \frac{2}{\pi} \int_0^\infty asy(t) \cos(\gamma b \cdot t) dt \tag{11}$$

It was therefore the object of my work to perform Fourier Transforms on the asymmetry data taken from the raw histogrammed data from the TRIUMF runs. Dr. Kossler and I did these four different ways: 1) Using a simple cosine transform, 2) Creating a fit to a group of coefficients a_i which are Fourier fit amplitudes, 3) Acknowledging the fact that the above a_i are components of a probability distribution which cannot go negative, and therefore creating a fit to e^{a_i}, 4) using a FORTRAN implementation of a Maximum Entropy technique. The technical details of each method are described below.

Each of the first three techniques is implemented in the TRI00 program. This program first prompts the user for the raw data file to be processed. The user then selects a packing factor, which determines the number of data points to be placed in each bin. As there are approximately 7700 points in each run, a packing factor of 15 was chosen to ensure approximately 500 units on the x-axis of the plots. The user must then select the pair of detectors (i.e. Front, Back, Left, Right) from which he or she wishes to derive the asymmetry. After selecting the detector pair, one must then input into TRI00 the value for alpha which appears in Eq. 8. This experimentally determined value was found to be 1.2567. The

program is now ready to calculate the asymmetry, which is done via the subroutine FF. While the name implies a Fast Fourier algorithm, it actually is just a simple cosine transform that produces the same results as the Fast Fourier Transform on real data, but the number of calculations it requires goes as n^2 whereas the FFT goes as $n \ln n$. Fortunately, the handling capacity of the CPUs that we used was great enough that the relative inefficiency of our algorithm to the FFT was on the order of a fraction of a second, and therefore negligible. This subroutine first generates the asymmetry data, and then dumps the asymmetry data to a file with three columns: time, asymmetry as a function of time, and the error in the asymmetry. One then must input the range of frequencies over which to perform the cosine transform algorithm. For our data, with ω measured in $\frac{Mrad}{s}$, ω_{start} was 0, ω_{end} was 40, and $n\omega$ was 80, implying that dω was .5. The algorithm then uses the following formula to compute the transform:

$$f(\omega_j) = \sum_i \cos(\omega_j \cdot t_i) \cdot asy(t_i) \tag{12}$$

which is analogous to Eq. 11 above. It should be noted that at this point in the program, one can manually input a first order phase correction, which for these data sets was found experimentally to be .5 *Mrad*. This phase correction is crucial to the absorption spectra. The second method that was used to calculate the Fourier Transform created a quantity, χ^2, which is shown below:

$$\chi^2 = \sum_i \frac{\left(asy(t_i) - \sum_j a_j \cdot \cos(\omega_j \cdot_i)\right)^2}{\sigma_i^2} \tag{13}$$

Here, the a_j are fit parameters which can be solved for numerically when we minimize χ^2 by setting $\frac{d\chi^2}{da_i} = 0$ and solving for the a_j . One noticeable aspect of Eq. 13 is that there is no requirement that the a_js should be positive. Consistent with this observation, plots of the a_js show negative values at several different points along the t-axis. These negative values are attributed to the background noise in the experiment. If the signal to noise is sufficiently large, the value of the a_js can be negative. But, because the field distribution is a *probability distribution*, it is important that we have a data set that represents what is physically allowable, i.e. positive. This forms the motivation for our third Fourier fit: the exponential fit. The exponential fits take the values of a_i's as starting points, then solve for a set of similar parameters, α_j, which are calculated by:

$$\chi^2 = \sum_i \frac{\left(asy(t_i) - \sum_j e^{\alpha_j} \cdot \cos(\omega_j \cdot_i)\right)^2}{\sigma_i^2} \tag{14}$$

This algorithm keeps the positive values fixed, but forces the negative values to go positive by placing them in the argument of the exponential. It then uses the fit procedure implemented via Eq. 13 above to find a better (positive) value.

The Maximum Entropy technique that we used as our fourth way of calculating the magnetic field distributions of the YBCO was implemented in a FORTRAN program. This program required data to be in a two-column form, where there were two parameters: time,

and some function of time that required data of the form

$$N(t) = N_0 \cdot \exp(-t/\tau_\mu) \cdot (1 + asy(t)) \tag{15}$$

N(t) above is similar in appearance to the raw histogrammed data initially recorded by the detectors in the TRIUMF setup: it is a decaying exponential that has a linear combination of sinusoidal oscillations in time superimposed over it. As the TRI00 program produced three-column asymmetry data, a short program was written to convert the asymmetry data produced by TRI00 into a form that the maximum entropy program could handle. This task was easily performed by the TRANSVERT program. TRANSVERT would take as its input the three-column data generated from each run in the TRI00 program and would produce as its output a two-column data file with two parameters: time and N(t) from Eq. 15 above. This change allowed the maximum entropy program to handle the μSR asymmetry data, and give us our fourth method of calculating the internal field distributions of the YBCO. See Figures 9 and 10.

Results and Discussions

The results of the four transforms for two data runs are displayed at the end of this paper. Run 936 was taken with an applied field of 102.2 G and a temperature of 75K. The applied field was almost entirely removed for run 947 (taken at .5 G), while the applied temperature was lowered to 18K. These two runs were picked on the basis of their interesting spectra, and several conclusions can be drawn from the figures shown below.

Several noteworthy aspects of the cosine transform can be seen in Fig. 3 and Fig. 4. After comparison with the other three methods, one notes a smoother shape of the field distribution, and a slight reduction in resolution. Both of these observations can be traced to the apodization factor which was introduced for the cosine transform.

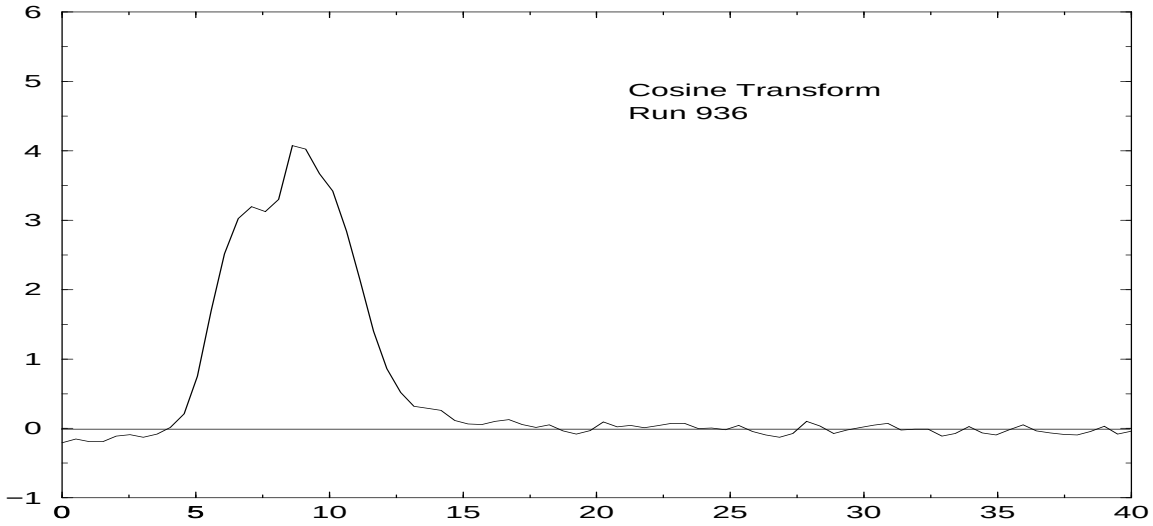

Figure 3: The cosine transform results for run 936

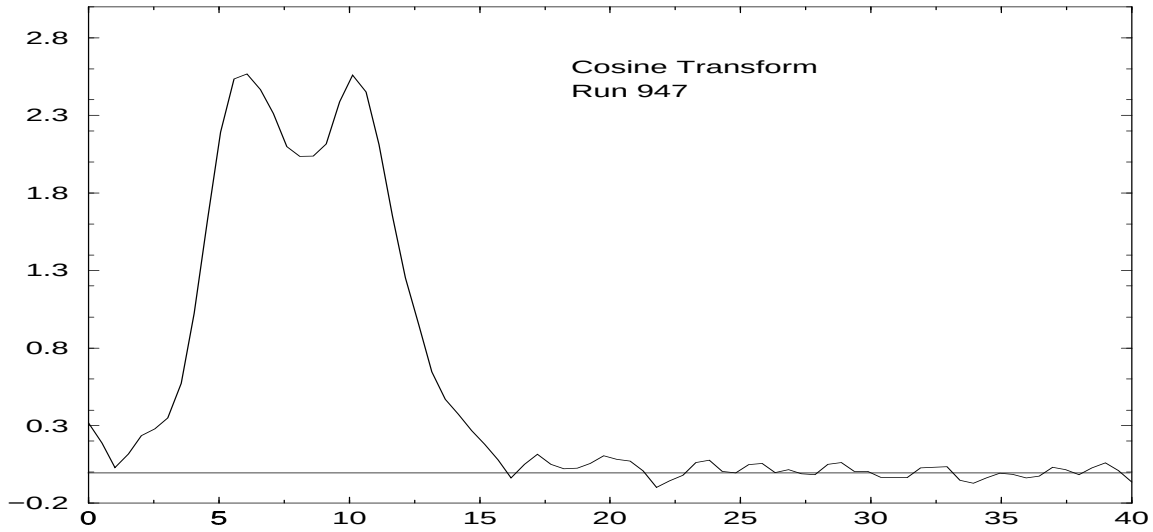

Figure 4: The cosine transform results for run 947

The fit to the Fourier amplitudes (Fig. 5 and Fig. 6) reveals a similar overall structure with perhaps higher resolution. For Run 936, this fit suggests the possibility of twin-peaked

structure which is not immediately apparent from the cosine transform. For Run 947, the two peaks of the spectra were more obvious initially. Components further away from the main spectra, however, remain present in both.

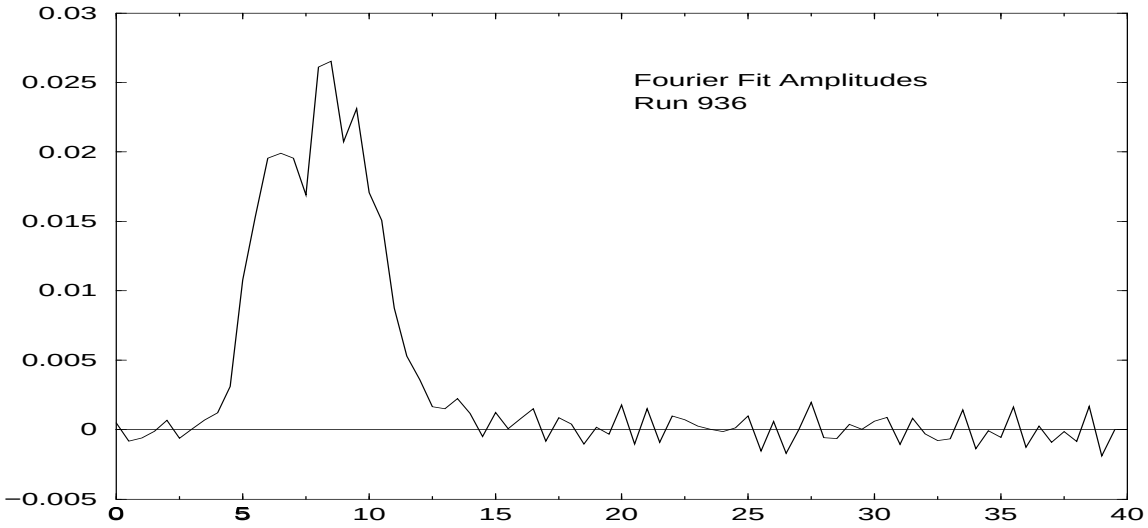

Figure 5: The fits a_j to the cosine amplitudes for run 936

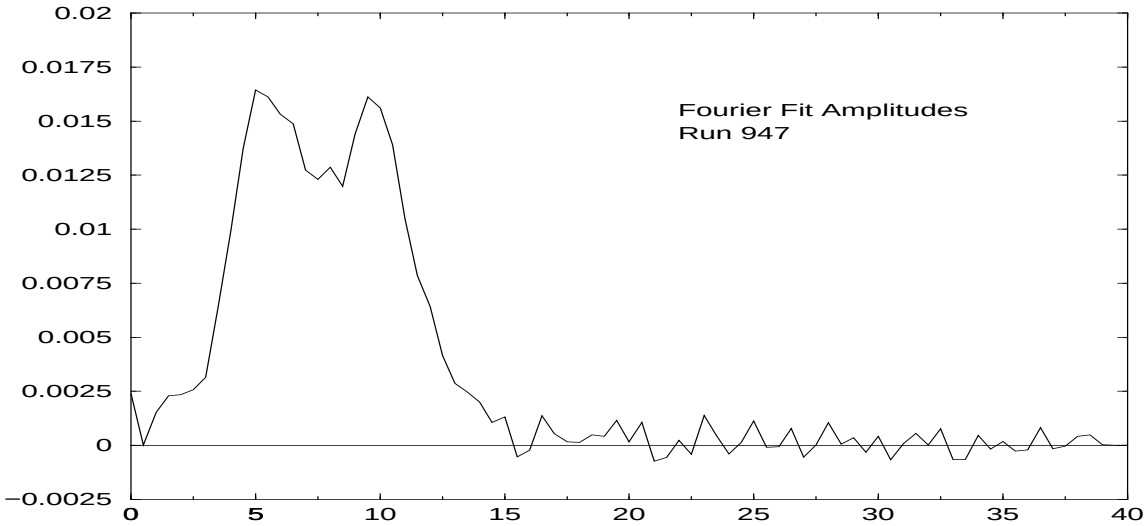

Figure 6: The fits a_j to the cosine amplitudes for run 947

The fits to the exponential amplitudes, Figs. 7 and 8, are obviously similar to their counterparts Figs. 5 and 6. No immediate additional knowledge is imparted from the study of these plots, although a possible use for the negative values of the original amplitude fits

is suggested later below.

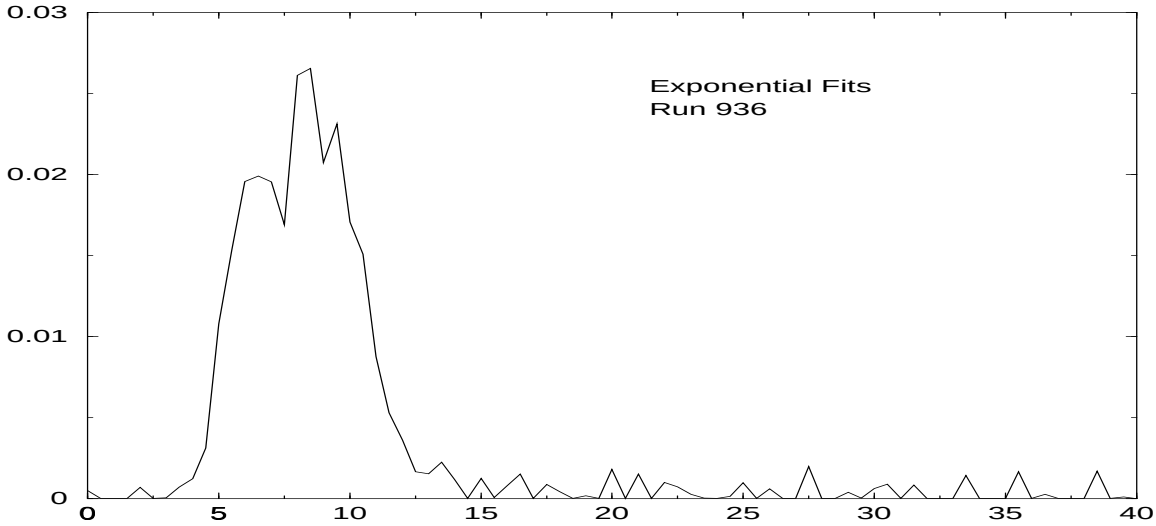

Figure 7: The exponential fits to the cosine amplitudes for run 936

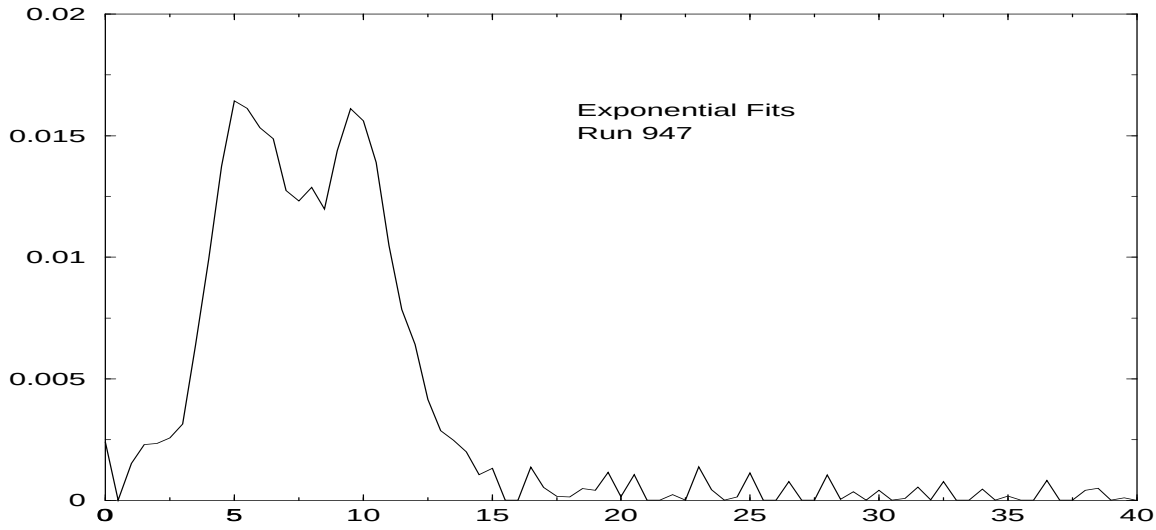

Figure 8: The exponential fits to the cosine amplitudes for run 947

Finally, the Maximum Entropy methods yielded Figs. 9 and 10. The additional structure between each of these diagrams' two peaks is indeed interesting. However, one is wary to conclude definitively that this additional structure exists. One should also note the virtual elimination of many of the components located further away from the main spectra that were present in the other three transformations.

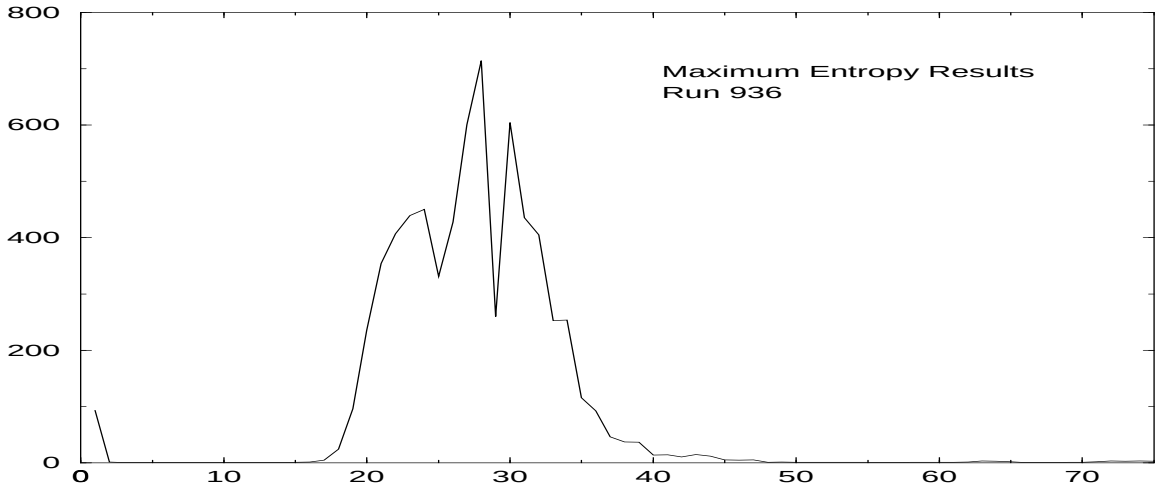

Figure 9: These are the maximum entropy amplitudes for run 936

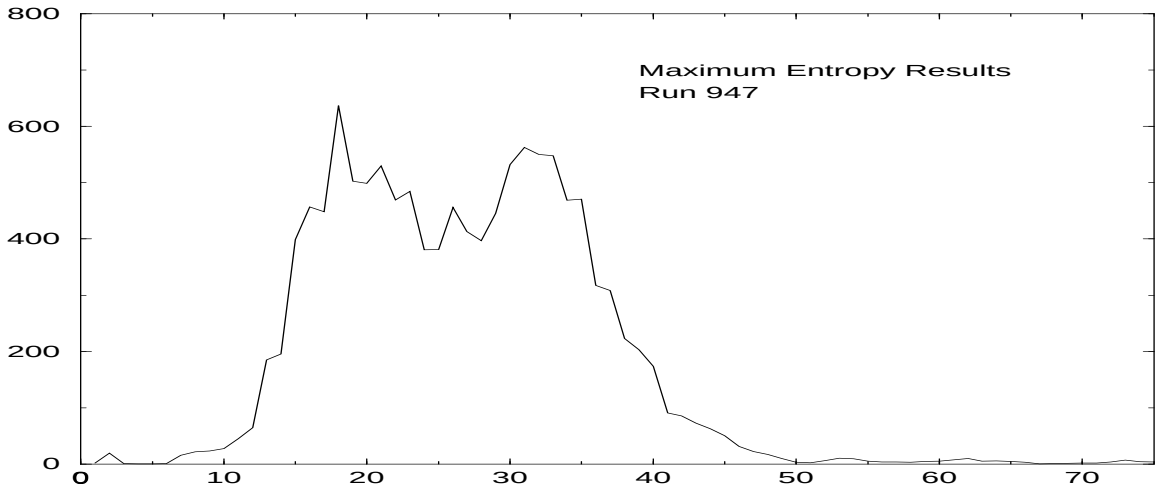

Figure 10: These are the maximum entropy amplitudes for run 947

Asymmetry of the Field Distribution and FLL Disorder

The data obtained from the Fourier transforms has several immediate applications. The first is the parameter α, which can be entirely determined (through its ω dependence) and is defined below:

$$\alpha = \frac{\sqrt[3]{\overline{(\omega - \overline{\omega})^3}}}{\sqrt{\overline{(\omega - \overline{\omega})^2}}} \tag{16}$$

It is known that α for a well-ordered lattice is large compared to that for a disordered one. As the longitudinal sections of these vortices stray away from being perfectly aligned, α is known to decrease. We therefore plan to use α as a means of quantifying the disorder or melting of the flux line lattice. Various means of obtaining the amplitude are needed to provide a measure of the systematic error in α.

Note that the negative components visible in the fit to the Fourier amplitudes may be useful, though unphysical. In calculating moments, the tendency of the poorly-known amplitudes at high ω will tend to cancel. On the other hand the corresonding amplitudes in the exponential fits and the Maximum Entropy fits all have positive signs.

It is our ultimate goal is to study the interesting and complicated spectra of a $Bi_2Sr_2CaCu_2O_8$ sample. This high purity sample shows marked narrowing of the field distribution at high fields. By studying the effects of the disorder through the skewness parameter α, it is hoped to separate the effects of disorder from the effects of the temperature dependence of the penetration depth. This latter is thought to reflect the underlying microscopic nature of the superconductivity.

References

[1] G. J. Bednorz and K. A. Müller. Possible high t_c superconductivity in the ba-la-cu-o system. *Z. Phys.*, B64:189, 1986.

[2] A. J. Greer and W. J. Kossler. *Low Magnetic Fields in Anisotropic Superconductors.* Springer Verlag, Berlin, 1995.

[3] J. H. Brewer. μssr, and introduction. http://musr.physics.ubc.ca/isms.

[4] P. G. de Gennes. *Superconductivity of Metals and Alloys.* Addison Wesley, 1989.

[5] Michael Tinkham. *Introduction to Superconductivity.* McGraw-Hill, 1995.

[6] M. K. Wu andJ. R. Ashburn, C. J. Torng, P. H. Hor, R. L. Meng, L. Gao, Z. J. Huang, Y. Q. Wang, and C. W. Chu. Superconductivity at 93 k in a new mixed-phase Yb-Ba-Cu-O compound system at ambient pressure. *Phys. Rev. Lett.*, 58:908, 1987.